related, spiral-like growth pattern on the surfaces of bulk $YBa_2Cu_3O_{7-\delta}$ ribbons (and occasionally on sintered pellets). Shown in Fig. 3 are scanning electron microscopy photographs from the surface of the ribbon sample. The appearance of spiral-like growth is evident in the figures, although the actual spirals are not as clearly defined and the step heights are much coarser (estimated to be about 10 to 100 nm within the resolution of the scanning electron microscope) than the unit-cell-high steps revealed by scanning tunneling microscopy (*1, 2*). These differences are attributed to the extensive coarsening of the structure in our samples after the long heat treatment of 940°C for 100 hours. The driving forces for the observed spiral-like growth may be the recrystallization and coarsening of severely strained and finely pulverized/smeared $YBa_2Cu_3O_{7-\delta}$ phase (caused by heavy cold rolling of the ribbons). The flat surface on each layer is believed to be the *a-b* plane along which the growth is known to be rapid.

The results in the present investigation imply that the dislocation density levels of 10^9 to 10^{10} cm^{-2} are not sufficient to explain the large difference in critical current densities between thin film and bulk Y-Ba-Cu-O. However, the dislocations remain as appealing pinning centers, as their core dimension is comparable to the coherence lengths in high T_c cuprate superconductors. Knowing that the density of dislocations can be significantly increased through materials synthesis and processing, as demonstrated by Hawley *et al.* (*1*) and Gerber *et al.* (*2*) as well as the present work, one of the possible approaches for significant pinning enhancement in high T_c superconductors may be to find practical techniques for increasing the density further by at least a few orders of magnitude.

REFERENCES

1. M. Hawley, I. D. Raistrick, J. G. Berry, R. J. Houlton, *Science* **251**, 1587 (1991).
2. C. Gerber, D. Anselmetti, J. G. Bednorz, J. Mannhart, D. G. Schlom, *Nature* **350**, 279 (1991).
3. S. Jin, T. H. Tiefel, G. W. Kammlott, *Appl. Phys. Lett.* **59**, 540 (1991).
4. S. Jin *et al.*, unpublished.
5. S. Nakahara, S. Jin, R. C. Sherwood, T. H. Tiefel, *Appl. Phys. Lett.* **54**, 1926 (1989).
6. C. P. Bean, *Rev. Mod. Phys.* **36**, 31 (1964).
7. M. Murakami *et al.*, *Cryogenics* **30**, 390 (1990).
8. B. Roas, L. Schultz, G. Saemann-Ischenko, *Phys. Rev. Lett.* **64**, 479 (1990).

14 May 1991; accepted 20 June 1991

Order and Disorder in C_{60} and K_xC_{60} Multilayers: Direct Imaging with Scanning Tunneling Microscopy

Y. Z. Li, M. Chander, J. C. Patrin, J. H. Weaver, L. P. F. Chibante, R. E. Smalley

Monolayer and multilayer structures of C_{60}, a high temperature van der Waals solid, have been studied with scanning tunneling microscopy. Structures grown on GaAs(110) at 300 kelvin and at elevated temperatures show significantly different morphologies because of balances between thermodynamics and kinetics. Condensation onto stepped surfaces demonstrates preferred bonding and nucleation at step edges. Detailed studies of potassium incorporation in crystalline C_{60} show highly ordered structures in the K_3C_{60} metallic state but disordered non-metallic structures for high potassium concentrations.

Recent breakthroughs (*1*) in the synthesis of C_{60} and related fullerenes (*2*) have made possible studies of the electronic (*3–5*), electrical (*6–9*), and structural (*10–16*) properties of these novel forms of carbon in pure and compound form. Structural transformations for pure C_{60} from face-centered cubic (fcc) to simple cubic (sc) have been observed upon cooling (*13*), and an fcc-bcc (body-centered cubic) tranformation has been reported upon reaction to form K_6C_{60} (*14*). Mobile hexagonal arrays of mixed C_{60} and C_{70} have been observed on Au(111), where surface interaction was very weak (*10*). Scanning tunneling microscopy (STM) results for C_{60} growth on GaAs(110) at 300 K revealed large stable monolayer islands and distinct adsorption sites (*11*). Variations in molecular height relative to the surface were related to the structure of the relaxed GaAs(110) substrate. It was not known, however, whether the bonding sites represented an equilibrium structure or one dictated by kinetics, that is, a growth structure. Since the spherical C_{60} molecule is bound by van der Waals interaction and desorbs in ultrahigh vacuum at ~550°C, C_{60} monolayers, multilayers, and solids offer unique opportunities to explore crystal growth driven by a simple interaction potential. The discovery of alkali metal incorporation into the fullerene lattice (*6–9*) raised questions as to the structure of thin films in the conducting and superconducting phase where ionic interactions were introduced.

This paper focuses on thin film structures of pure and K-doped C_{60} grown on GaAs(110). With STM, we have examined C_{60} monolayers and multilayers prepared at temperatures from 300 K to 470 K. The results show that ordered C_{60} structures can be commensurate or incommensurate with the substrate. Multilayer growth at 300 K produces growth structures with point defects, dislocations, domain boundaries, and surface faceting. Multilayer C_{60} growth at 470 K yields structures that are almost per-

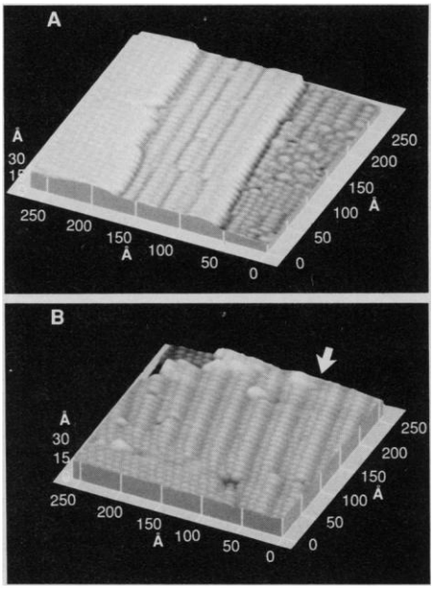

Fig. 1. STM images of kinetically limited C_{60} multilayer growth structures at 300 K. Image (**A**) reveals first, second, and third layers, while (**B**) focuses on an area of the third layer. Row-like structures in (A) run along the [1$\bar{1}$1] direction of the substrate, and they expose mainly (311) and (211) faces of the fcc lattice in which the (111) terrace normals are not perpendicular to the surface. The sawtooth structure at the center of (B) consists of (211) and (533) faces, the latter indicated by an arrow. The lower left corner shows a (111) close-packed face.

Y. Z. Li, M. Chander, J. C. Patrin, J. H. Weaver, Department of Materials Science and Chemical Engineering, University of Minnesota, Minneapolis, MN 55455.
L. P. F. Chibante and R. E. Smalley, Rice Quantum Institute and Departments of Chemistry and Physics, Rice University, Houston, TX 77251.

fectly ordered. Growth on stepped surfaces demonstrates enhanced bonding and island nucleation at step edges. The incorporation of K produces well-ordered, metallic K_xC_{60}, $x \cong 3$. Continued K incorporation produces non-metallic structures that exhibit substantial disorder.

The fullerenes were formed by the contact arc method (*17*), with subsequent separation by solution with toluene. Phase-pure C_{60} was obtained by a liquid chromatography process on alumina diluted with mixtures of hexanes. The resulting fullerenes were rinsed in methanol, dried, and sublimed in the ultrahigh vacuum STM chamber onto substrates held at temperatures between 300 K and 470 K. The pressure remained below 1×10^{-9} torr during thin film growth. The operating pressure was ~6×10^{-11} torr. The amount of material deposited was measured with a quartz crystal thickness monitor. Alkali metal depositions were done using a SAES dispenser ~5 cm from the sample. GaAs(110) surfaces were prepared by cleaving in situ. Length scales were calibrated with the GaAs(110) lattice and with substrate monatomic steps. The images were not corrected for thermal drift or piezo creep. The STM images were acquired while probing either occupied or unoccupied states. A bias voltage in the range of ±(1.7 to 3.0) V was typically used for imaging pristine fullerene films.

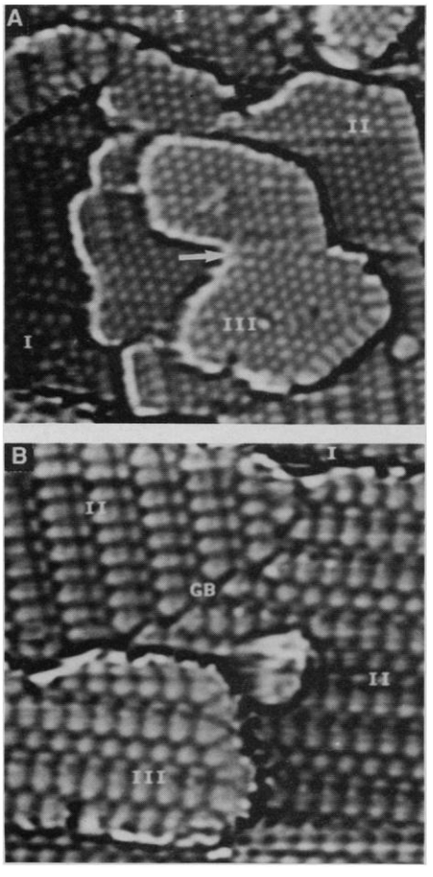

Fig. 2. Curvature-enhanced images that reveal C_{60} growth structures of the first three layers labeled I, II, and III. The arrow in (**A**) indicates a grain boundary between two close-packed regions in the third layer. A grain boundary (GB) in the second layer between two mainly (311) regions is shown in (**B**).

The molecular adsorption structure for the first monolayer of C_{60} on GaAs(110) was discussed by Li *et al.* (*11*). As a C_{60} multilayer is formed, the surface structure becomes more complex. This is especially true for films grown at 300 K because there are a large number of inequivalent structures in these films. Figure 1 shows STM images acquired after the deposition of ~1 monolayer of C_{60} on GaAs(110) at 300 K. The substrate $[1\bar{1}0]$ direction for the images presented here is from the lower right to the upper left. Islands of multilayer C_{60} were formed, and Fig. 1 reveals C_{60} islands with thicknesses up to three monolayers. The steps separating different layers are ~7 Å in height, consistent with close packing. Step edges consist of straight segments, suggesting that growth proceeds along a front with a close-packed structure and molecular accommodation is favored at kink sites. Figure 1A depicts the first, second, and third monolayers and Fig. 1B emphasizes a third layer region. The corrugated row-like structures in the second layer are oriented along the substrate $[\bar{1}1\bar{1}]$ direction. The third layer in Fig. 1A demonstrates that, on occasion, a C_{60} layer grown on a corrugated layer can be free of such corrugation. Such compensation of corrugation with additional molecular layers illustrate the complexity of stacking at 300 K. One can speculate that growth at low temperature of other van der Waals solids with spherical elements will produce equivalent structures.

Flat and corrugated regions can coexist, as shown in Fig. 1B, in a third layer island. The lower left region has a distorted close-packed structure while the remainder has a corrugated structure. Close examination of the corrugated region shows it to be a faceted surface with high Miller indices resembling a sawtooth-like surface. Figure 1B then represents a (211) face of the fcc structure with (111) terraces pointing away from the surface normal. The arrow in Fig. 1B points to the region where the sawtooth periodicity is interrupted, resembling a (533) stripe, probably with the (111) terrace inclined differently from the other terraces shown.

Grain boundaries within a two-dimensional (2D) C_{60} layer can be found between corrugated and flat regions or between corrugated regions. A typical boundary between a flat and a corrugated region is shown at the lower right of Fig. 2A; a boundary between two corrugated regions can be seen in Fig. 2B. The upper left region of Fig. 2B has (311) surface structure while the lower right region is a mixture of (311) and (211). A boundary between two flat regions is also evident in the third layer near the center of Fig. 2A. The existence of such 2D grain boundaries indicates that C_{60} monolayer islands have nucleated separately and grown together. Typically, an extra layer grown on a flat or a corrugated region

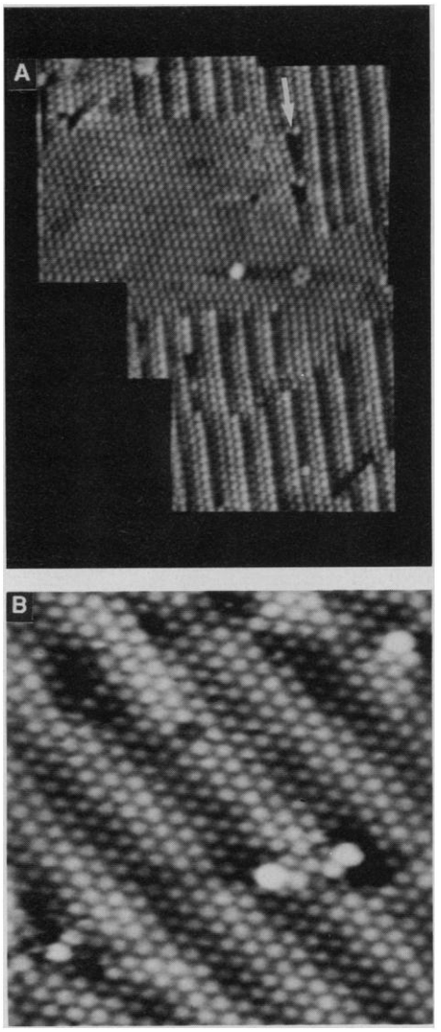

Fig. 3. (**A**) An STM mosaic for a C_{60} bilayer. The corrugated or sawtooth structure and the flat region in the center are characteristic of multilayers prepared at 450 K. The flat region has a close-packed (111) surface of the fcc lattice while the corrugated regions are comprised of (211) and (533) faces. The arrow draws attention to a low-angle grain boundary. (**B**) Incommensurate monolayer growth of C_{60} on GaAs(110) at 450 K produces a ripple-like structure in which the bright and dark bands reflect height modulations as the molecules fall in and out of phase with the substrate corrugation.

maintains the structure of the underlying layer, as depicted in Fig. 2, but Fig. 1A serves as a counter-example. It is not clear whether 2D grain boundaries propagate through 3D overlayers, but Fig. 2 suggests such propagation.

Thermodynamic factors related to substrate bonding and the bulk C_{60} growth energetics are important in the formation of corrugated high-index surfaces like those discussed above but kinetic factors should also be considered. To determine whether structures grown at 300 K were kinetically constrained, we studied samples grown or annealed at higher temperatures. Figure 3A shows a mosaic of STM images for a C_{60} bilayer grown on GaAs(110) at 450 K. Two distinct structures can be identified. Corrugated regions are evident in the upper and lower parts as a mixture of (211) and (533) faces of the fcc surface, as in Fig. 1B. In contrast, the central region is a flat area with perfect lateral alignment among C_{60} molecules with row directions that are no longer determined by the substrate $[1\bar{1}1]$ and $[\bar{1}1\bar{1}]$ directions. In addition, the equivalent of a low-angle grain boundary is evident (indicated by an arrow) in the upper right quadrant as the flat region joins the corrugated region. One extra row is inserted after six molecules, giving an angle of ~10°.

The corrugated structures of Figs. 2 and 3A represent typically (211) surfaces, and their formation would seem energetically costly compared to close-packed (111) faces. Nevertheless, they form at 300 K and 450 K. However, when four- to six-monolayer C_{60} films were grown at 470 K the typical island size was much larger than shown in Fig. 3A and the corrugated regions were strikingly absent. Therefore, we postulate that for growth at 300 K, a tilted close-packed structure seems favorable due to the strain in the first monolayer, and this structure propagates to the multilayer surface to form (211) and (311) facets. Growth at 470 K, however, produces a uniform first monolayer so that additional layers adopt the thermodynamically favored (111) orientation.

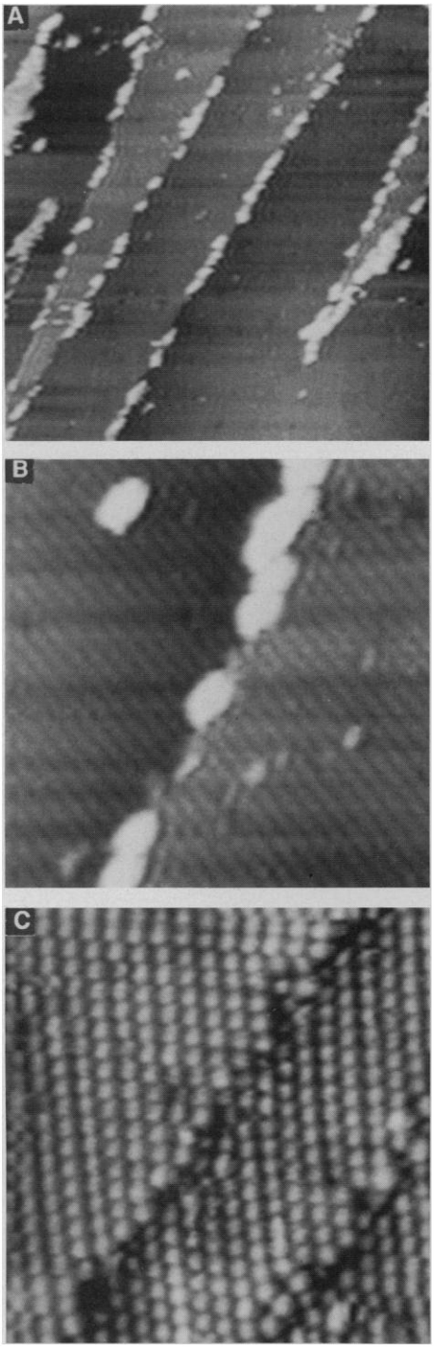

Fig. 4. Image (**A**) demonstrates enhanced accommodation of C_{60} molecules at monatomic step edges of the GaAs substrate. The image size of (A) is 700 × 700 Å^2. Image (**B**) shows an area of 160 × 160 Å^2. With higher resolution, the As rows of the substrate can be imaged (separated by 5.65 Å), and individual C_{60} molecules are seen to decorate the step with elongation related to tip-effects. With increasing coverage, the monolayer film follows the substrate step structure. Image (**C**) shows two monatomic steps running diagonally through the image.

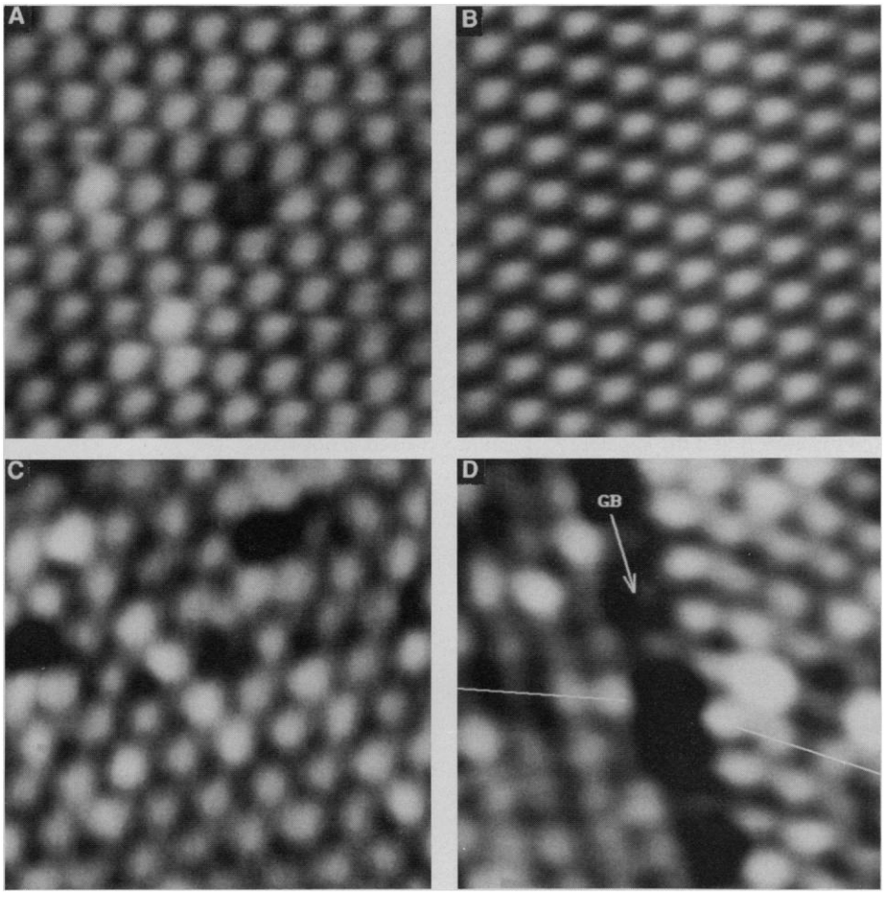

Fig. 5. Image (**A**) reveals the surface structure of a C_{60} film prepared at 470 K. The close-packed structure remained unchanged after potassium deposition, as shown in (**B**), and the film was metallic with stoichiometry close to K_3C_{60}. A doubling in deposition produced a non-metallic film with numerous defects and disordered protrusions. Even the flat regions were characterized by differences in the brightness of the molecules, as shown in (**C**), perhaps because of different potassium coordination. Grain boundaries (GB) were also observed between regions with different molecular alignment, as shown in (**D**).

Figure 3B shows a ripple structure that was often observed for the flat regions of the first monolayer or even the second monolayer C_{60}. The C_{60} monolayer depicted was grown at 450 K prior to cooling to 300 K for imaging. The average distance between ripples is ~45 Å along the substrate [001] direction (lower left to upper right of the image). This indicates an incommensurate growth structure. Along the [001] direction, C_{60} molecules fall in-phase and out-of-phase with the corrugation of the relaxed GaAs(110) surface with height differences determined by the surface. An estimate of the period based on the lattice mismatch gives the distance between ridges to be ~45 Å and the peak-to-valley height ~0.8 Å, in excellent agreement with measurements from Fig. 3B.

The bonding of C_{60} molecules to GaAs(110) is van der Waals in character and the preference of one site over another is rather weak, as can be seen in the incommensurate structure of Fig. 3B. However, one would expect this interaction to be enhanced at substrate steps due to different structural configurations. Although an atomic step on GaAs(110) is only 2 Å high, the ability of the step to enhance molecular sticking is obvious from Fig. 4A, which is a stepped surface onto which submonolayer C_{60} had been condensed at 410 K with post-deposition annealing at 470 K. While flat regions of the surface were essentially free of C_{60}, molecular decoration of the steps was evident. Higher resolution images, as in Fig. 4B, revealed that substrate steps were decorated by one or two rows of C_{60} parallel to the step direction. Note that these images are overexposed to show the substrate arsenic rows; the spacing between rows is 5.65 Å and the apparent elongation of the bright C_{60} features is possibly a tip-shape effect from imaging individual molecules. Occasionally, large islands of C_{60} were imaged that appeared to nucleate along the steps.

When the C_{60} coverage of the stepped surface was increased, the steps between the upper and lower terraces were clearly evident by the structural discontinuity and height of the stepped C_{60} layers. Figure 4C depicts two C_{60}-covered GaAs(110) steps on a monolayer surface prepared at 410 K. The uniformity of the C_{60} film on the central terrace shows that it is a single domain. This indicates C_{60} layer growth by "step flow" because molecular accommodation at the step edge is large, and island nucleation on the terrace is suppressed.

The observation of superconductivity in the K_xC_{60} fulleride raises questions about the electronic states and the structure of the solid. All indications are that the potassium atoms occupy the tetrahedral and the octahedral interstitial sites in the fcc C_{60} structure to produce K_3C_{60} (*5, 7, 16*). For ideal K_3C_{60}, the degenerate bands derived from the lowest unoccupied molecular orbital (LUMO) of the fullerene would be half-occupied (*7*). A recent x-ray diffraction study demonstrated that a fully reacted phase, K_6C_{60}, is characterized by a bcc lattice with K atoms that form a cross-like structure at the center of the {100} faces of the unit cell, that is, offset tetrahedral sites of the bcc lattice (*14*).

Figure 5 shows a series of STM images for 5 ML C_{60} before and after exposure to potassium. The regular lattice prepared at 470 K, Fig. 5A, was routinely observed with bias voltages between 2 V and 2.8 V. These surfaces were very flat and were well ordered, and the tunneling tips were stable. Significantly, they remained well ordered after potassium incorporation to form the metallic fulleride. Figure 5B shows the surface of a perfect lattice obtained after the sample had been exposed to the potassium flux for 30 min, a condition that yielded states at the Fermi level that were derived from the lowest unoccupied molecular level of the isolated molecule (*5*). The metallic character of the multilayer was evident from *I-V* measurements: bias voltages of only 0.01 to 0.3 V were used to acquire images such as that shown in Fig. 5B. The absence of lattice transformation or disorder introduced by potassium atom incorporation is consistent with potassium occupation of tetrahedral and octahedral sites of the fcc lattice to produce K_3C_{60}, a process favored by ~1.1 eV per ion (*5*). The absence of potassium-related features reflects the fact that potassium is fully ionized and the empty *s*-band is not accessed.

With increased potassium incorporation, it became increasingly difficult to image the surface, and the tips were easily damaged by numerous surface protrusions. Figure 5C shows a flat region characteristic of areas between these mostly disordered protrusions for a film prepared by 60-min exposure to potassium at 470 K (double that of Fig. 5B). A bias voltage of ~2 V was necessary to effect tunneling from the sample to the tip. This demonstrates that additional potassium incorporation caused the overlayer to evolve into a non-metallic state, and tunneling involved the now filled LUMO-derived band of the fulleride (*5*). Heavily potassium-doped K_xC_{60} films prepared at 300 K showed higher degrees of disorder, and flat regions like Fig. 5C were difficult to locate. The brightness of the individual C_{60} features was also very nonuniform, an effect we attribute to different coordination of potassium with the C_{60} molecules of the lattice, that is, potassium lattice disorder. Filling of the tetrahedral sites of the bcc lattice would produce non-metallic K_6C_{60}, but the irregular surface layer would exhibit less complete K-C_{60} coordination. Indeed, the potassium geometry cannot be determined by the present STM study. Although molecular rotation is expected to be impeded by the attachment of potassium atoms, there was no evidence of C_{60} internal structure.

The heavily doped K_xC_{60} films also exhibited different local crystal orientations and possibly different structures. (Such effects were not observed for the K_3C_{60} surface.) They can be best demonstrated by the appearance of a grain boundary, as shown in Fig. 5D. The right side of this image showed the same structure as that in Fig. 5C but the C_{60} rows on the left side were aligned along a different direction. This, and the surface disorder discussed above, probably reflect the structural transformation from fcc to bcc (*14*). The presence of grain boundaries indicates multiple nucleation sites for the bcc lattice. The close-packed (110) face of the bcc crystal resembles the distorted (111) face of the fcc structure, and it is possible to distinguish these two structures using STM with certainty only when the stacking geometry can be determined at single height steps. This has not yet been possible.

These STM studies of C_{60} show equilibrium and nonequilibrium structures for growth in the temperature range $300 \leq T \leq 470$ K. These are the first direct images of multilayer structures of a van der Waals solid, and they demonstrate complex order and disorder due to kinetic constraints. Again, it would seem that the fullerenes offer unique opportunities to explore fundamental physical phenomena, in this case because the bond strength is much greater than for other van der Waals solids. Indeed, the desorption temperature of C_{60} suggests that the cohesive energy is about eight times that of Xe, namely ~1.35 eV. The results show stable bonding structures on the surface and long-range-ordered monolayer formation when kinetically permitted. Growth at 300 K produces ordered multilayers with defects, dislocations, grain boundaries, and surface faceting.

REFERENCES AND NOTES

1. W. Krätschmer, L. D. Lamb, K. Fostiropoulos, D. R. Huffman, *Nature* **347**, 354 (1990).
2. H. W. Kroto, J. R. Heath, S. C. O'Brien, R. F. Curl, R. E. Smalley, *ibid.* **318**, 162 (1985).
3. D. L. Lichtenberger, K. W. Nebesny, C. D. Ray, D. R. Huffman, L. D. Lamb, *Chem. Phys. Lett.* **176**, 203 (1991).
4. J. H. Weaver *et al.*, *Phys. Rev. Lett.* **66**, 1741 (1991); M. B. Jost *et al.*, *Phys. Rev. B.*, in press.
5. P. J. Benning, J. L. Martins, J. H. Weaver, L. P. F. Chibante, R. E. Smalley, *Science* **252**, 1417 (1991).

6. R. C. Haddon *et al.*, *Nature* **350**, 320 (1991).
7. A. F. Hebard *et al.*, *ibid.*, p. 600.
8. K. Holczer *et al.*, *Science* **252**, 1154 (1991).
9. M. J. Rosseinsky *et al.*, *Phys. Rev. Lett.* **66**, 2830 (1991).
10. R. J. Wilson *et al.*, *Nature* **348**, 621 (1990); J. L. Wragg, J. E. Chamberlain, H. W. White, W. Krätschmer, D. R. Huffman, *ibid.*, p. 623.
11. Y. Z. Li *et al.*, *Science* **252**, 547 (1991).
12. R. M. Fleming *et al.*, *Mat. Res. Soc. Symp. Proc.*, in press.
13. P. A. Heiney *et al.*, *Phys. Rev. Lett.* **66**, 2911 (1991).
14. O. Zhou *et al.*, *Nature* **351**, 462 (1991).
15. J. M. Hawkins, A. Meyer, T. A. Lewis, S. Loren, F. J. Hollander, *Science* **252**, 312 (1991).
16. P. W. Stephens *et al.*, *Nature* **351**, 632 (1991).
17. R. E. Haufler *et al.*, *J. Phys. Chem.* **94**, 8634 (1990).
18. This work was supported by the Office of Naval Research, the National Science Foundation, and the Robert A. Welch Foundation. Discussions with J. L. Martins are gratefully acknowledged, as is the ongoing cheerful support of Park Scientific Instruments.

28 May 1991; accepted 19 June 1991

Density-Dependent Natural Selection and Trade-Offs in Life History Traits

LAURENCE D. MUELLER, PINGZHONG GUO,* FRANCISCO J. AYALA

Theories of density-dependent natural selection state that at extreme population densities evolution produces alternative life histories due to trade-offs. The trade-offs are presumed to arise because those genotypes with highest fitness at high population densities will not also have high fitness at low density and vice-versa. These predictions were tested by taking samples from six populations of *Drosophila melanogaster* kept at low population densities (*r*-populations) for nearly 200 generations and placing them in crowded cultures (*K*-populations). After 25 generations in the crowded cultures, the derived *K*-populations showed growth rate and productivity that at high densities were elevated relative to the controls, but at low density were depressed.

ONE OF THE FIRST SUCCESSFUL combinations of theory from ecology and evolution was the theory of density-dependent natural selection, often called *r*- and *K*-selection, where *r* and *K* refer to low- and high-density conditions, respectively (*1*). The initial models combined theoretical models of population growth dynamics with single-locus population genetic models in order to describe evolution in environments that differ with respect to population density (*2*); more complex elaborations of these early models were advanced later (*3*). These theories and models have assumed a central role in the theory of evolutionary ecology (*4*). A crucial assumption of these theories has been that genotypes selected for sustained reproduction and survival at high population densities are not likely to do as well at low densities; likewise organisms capable of rapid reproduction under low levels of crowding may not reproduce as well under crowded conditions. It has been, however, difficult to demonstrate empirically the postulated trade-offs (*5*).

We have previously shown (*6*) that three populations of *Drosophila melanogaster* kept at low density (*r*-populations) had, after eight generations, higher rates of population growth when tested at low densities than three populations kept at high density (*K*-populations), whereas the opposite was the case for growth rates tested at high population densities. The interpretation and significance of these results were complicated by three issues. (i) Given that both the low- and high-density environments were novel for these populations, it remains possible that the differences observed between the *r*- and *K*-populations were not due to changes in both populations but rather that only one population had evolved whereas the other retained the attributes of the founder population. (ii) The differences observed between *r*- and *K*-populations with respect to growth rates and total productivity at low density were only marginally significant. (iii) No additional tests have been carried out to verify these results; indeed one study of mosquitoes from natural populations did not show any trade-off in population growth rates (*7*).

We describe an experiment designed to overcome these problems, the results of which confirm that trade-offs do occur in the evolution by density-dependent natural selection. We test two types of high density populations (*rK*- and *r*×*rK*-populations), both derived from *r*-populations now transferred to the *K*-environment; the controls are two types of low density populations (*r*- and *r*×*r*-populations) (Fig. 1). The *r*×*r*-populations were created to introduce genetic variation into replicate sets of low density populations. The *rK*-populations were created from samples of each *r*-population and had been maintained at high densities for 25 generations prior to this experiment. In a similar fashion the *r*×*rK*-populations are samples from the *r*×*r*-populations that have been kept at high densities.

Each of the four types of populations consisted of three replicates. During the course of this experiment the *r*- and *r*×*r*-populations are not expected to change significantly, given that they had been previously kept for nearly 200 generations at the same low density as now. However, the *rK*- and *r*×*rK*-populations have been transferred from the low density *r*-environment to the high density *K*-environment. Hence, differences that arise between them and the *r* and *r*×*r* controls may be attributed to adaptation to the new high-density environments.

After the three *rK*- and three *r*×*rK*-populations had undergone 25 generations of natural selection in their new environments, we measured rates of population growth and net productivity in each of these six

Table 1. The mean values (and standard errors) for productivity and growth rate for each population and each density.

Population	Productivity (no. of adults) by density			Growth rate (no. of offspring per adult per week) by density		
	10	750	1000	10	750	1000
r_1	872 (52)	739 (24)	817 (17)	5.58 (0.20)	1.53 (0.017)	1.40 (0.021)
r_2	917 (16)	800 (38)	808 (20)	6.01 (0.16)	1.55 (0.03)	1.43 (0.0075)
r_3	788 (21)	770 (47)	797 (45)	5.05 (0.19)	1.47 (0.033)	1.37 (0.019)
rK_1	834 (26)	784 (24)	858 (67)	5.69 (0.10)	1.51 (0.015)	1.43 (0.029)
rK_2	799 (22)	856 (9)	935 (23)	5.19 (0.17)	1.52 (0.009)	1.45 (0.012)
rK_3	725 (41)	852 (14)	948 (33)	5.09 (0.15)	1.52 (0.0031)	1.43 (0.0092)
$r \times r_1$	736 (20)	689 (28)	823 (20)	5.54 (0.12)	1.43 (0.016)	1.37 (0.0044)
$r \times r_2$	772 (28)	745 (24)	846 (52)	5.16 (0.095)	1.42 (0.0088)	1.37 (0.022)
$r \times r_3$	774 (16)	743 (10)	822 (61)	5.38 (0.12)	1.41 (0.0048)	1.35 (0.026)
$r \times rK_1$	680 (19)	773 (24)	862 (18)	5.13 (0.037)	1.45 (0.0062)	1.40 (0.011)
$r \times rK_2$	699 (32)	804 (18)	952 (47)	5.11 (0.10)	1.44 (0.012)	1.41 (0.026)
$r \times rK_3$	667 (32)	799 (38)	944 (24)	4.98 (0.12)	1.45 (0.017)	1.39 (0.0031)

Department of Ecology and Evolutionary Biology, University of California, Irvine, CA 92717.

*Present address: Department of Biology, Beijing Teachers College, Beijing 100037, China.